Lasers Med Sci (2013) 28:1323–1329
DOI 10.1007/s10103-012-1245-6

ORIGINAL ARTICLE

Comparison of elastic scattering spectroscopy with histology in ex vivo prostate glands: potential application for optically guided biopsy and directed treatment

O. M. A'Amar · L. Liou · E. Rodriguez-Diaz · A. De las Morenas · I. J. Bigio

Received: 24 April 2012 / Accepted: 4 December 2012 / Published online: 18 December 2012

Abstract The false-negative rate of ultrasound-guided sextant prostate biopsy has been estimated to be as high as 35 %. A significant percentage (10–35 %) of these prostate cancers diagnosed at a second or later attempt are high grade and, therefore, potentially lethal. We discuss the feasibility for performing optically guided biopsy using elastic scattering spectroscopy (ESS) to reduce sampling errors and improve sensitivity. ESS measurements were performed on 42 prostate glands ex vivo and correlated with standard histopathological assessment. Sliced glands were examined with wavelength ranges of 330–760 nm. The ESS portable system used a new fiber-optic probe with integrated cutting tool, designed specifically for ex vivo pathology applications. ESS spectra were grouped by diagnosis from standard histopathological procedure and then classified using linear support vector machine. Preliminary data are encouraging. ESS data showed strong spectral trends correlating with the histopathological assignments. The classification results showed a sensitivity of 0.83 and specificity of 0.87 for distinguishing dysplastic prostatic tissue from benign prostatic tissue. Similar results were obtained for distinguishing dysplastic prostatic tissue from prostatitis with a sensitivity and specificity of 0.80 and 0.88, respectively. The negative predictive values obtained with ESS are better than those obtained with transrectal ultrasound (TRUS)-guided core-needle biopsy.

Keywords Optical spectroscopy · Cancer · Pathology · Prostate · Fiber-optic probe

O. M. A'Amar (✉) · E. Rodriguez-Diaz · I. J. Bigio
Department of Biomedical Engineering, Boston University, Boston, MA 02215, USA
e-mail: oaamar@bu.edu

L. Liou
Cambridge Health Alliance, Harvard Medical School, Cambridge, MA, USA

L. Liou · A. De las Morenas
Department of Pathology, Boston University Medical Center, Boston, MA, USA

Introduction

Prostate cancer is the most commonly diagnosed cancer among men in the USA and is the second cause of cancer-related death among this population. However, if prostate cancer is detected in its early stage, it can be effectively treated and cured. Digital rectal examination (DRE) and prostate-specific antigen (PSA) measurement are the methods used by clinicians in screening for prostate cancer. However, the ability of DRE to detect early-stage prostate cancer is limited. PSA is also not ideal because this enzyme can rise naturally in men as they age or in other benign prostate diseases such as prostatitis. PSA cannot distinguish prostate cancer from normal growth or other benign conditions. The definitive diagnostic method for prostate cancer currently relies on histopathology assessment following a transrectal ultrasound (TRUS)-guided core-needle biopsy. This procedure is prompted either by an elevated serum PSA level or a palpable nodule. The prostate biopsy also has limitations due to the biopsy procedure. Ultrasound imaging of prostate cancer is not sensitive enough to detect cancer but is used only to guide the needle to areas of the prostate. This means that all prostate biopsies typically 6–12 are not targeted but random and false-negative rates can be high.

In a multicenter clinical trial [1], in which 6,630 men were screened with PSA and TRUS, an abnormality on TRUS defined as a hypoechoic region corresponded to prostate

cancer in only 18 % of the cases. Conversely, 65 % of non-malignant appearing regions on TRUS (i.e., isoechoic) were found to contain adenocarcinoma of the prostate. The study concluded that 52 % of men diagnosed with prostate cancer would have been missed if only the hypoechoic lesion was biopsied. As a result, biopsy of the hypoechoic lesion alone is not sufficient. Therefore, directed biopsies are sometimes obtained when a palpable nodule is noted on digital rectal examination and more biopsies have been suggested to generate a higher yield in men with larger (> 30 cm^3) prostate glands [2–4].

Approximately 66 % of patients, who have an elevated PSA (> 4 ng/ml), will have a negative biopsy following an ultrasound-guided sextant sampling [3, 5–7]. It is thought that the basis of the sampling error is that an 18-gauge biopsy core samples a 1-mm diameter of tissue over the prostatic rectal interface whose surface area is approximately 30×30 mm in the case of a normal size gland (prostate gland volume 25–30 cm^3). Therefore, despite six samples only a 2-×3-mm region (6 mm^2/900 mm^2) corresponding to ~1 % of the entire surface area is sampled and investigated. In addition, the core length is typically 1.0–1.5 cm, which at best samples 50 % of the anterior to posterior extent of the cancer bearing region of the prostate gland (i.e., peripheral zone). It has been estimated that the false-negative rate of a standard sextant sampling ranges from 15–31 % [1–4]. Most important, however, is the observation that a significant minority (10 %–35 %) of these prostate cancers diagnosed at a second or later attempt are high grade (Gleason score 7 or higher) and therefore, potentially lethal [3, 5–7]. This delay in diagnosis due to sampling error can impact prognosis in some patients.

Optical techniques promise to provide real-time information in situ, without the need to excise and process specimens. By combining optimized optical guidance with core biopsy, the sampling errors inherent in core biopsy could be significantly reduced, improving the sensitivity and reducing false negatives. Optical "biopsy" measurements can be conducted through very fine needles (as small as 25-gauge) and thus can be integrated with core biopsies to reduce sampling error and improve sensitivity. Alternatively, optical assays with a fine needle can precede and provide guidance for core biopsies. This results in reduced trauma from multiple excisions of core specimens. Moreover, continuous measurement can be performed over the entire insertion track of the needle, from the entrance surface to the opposite side of the capsule. Thus, a much larger range of sites can be assessed in the gland, with reduced trauma compared with TRUS-guided core biopsies. The above procedure may cause blood contamination effect. However, moving the needle slightly and/or changing the location, by pushing the probe tip through any blood to directly contact the tissue typically helps reduce the effect of blood contamination. Although the sampled volume by optical "biopsy" techniques is still small (~1 % of the total gland volume), this technique when associated with TRUS has the potential to provide real-time diagnostic signatures.

Optical techniques offer a range of modalities for diagnosis, and include elastic scattering spectroscopy (ESS), laser-induced fluorescence spectroscopy [8–11], optical coherence tomography [9, 12], and Raman spectroscopy [13–15]. ESS is distinguished from diffuse-reflectance spectroscopy [16], in that the source-detector separation for ESS is small—much less than the scattering mean free path. ESS is a particularly attractive technique since it provides spectra that contain information about the sub-cellular morphology of the tissue as well as the chromophore content (e.g., hemoglobin and melanin) [17]. Because ESS translates tissue morphological changes at the cellular and sub-cellular level into spectral features [18], it can be correlated with standard histopathologic assessment, which is commonly based on the analysis of microscopic structure [19]. Hence, ESS may be an appropriate technique for prostate cancer diagnosis, with the advantage of providing minimally invasive real-time diagnostic signatures in situ, which are related to histopathology.

Salomon et al. have conducted an ex vivo study in which 95 liquid nitrogen frozen tissue samples, from 32 patients undergoing radical prostatectomy for clinically localized prostate cancer, were studied using a triple spectroscopy technique (laser-induced autofluorescence, white-light remission (ESS), and high-frequency impedance spectroscopy) [15]. They reported promising statistics of detecting prostate cancer. A combination of laser-induced autofluorescence and white-light remission data demonstrated a differentiation of benign and malignant prostate tissue with a sensitivity of 87.5 % and a specificity of 87.3 %. These numbers improved to 93.8 % sensitivity and 92.4 % specificity when the data collected from high-frequency impedance was included in the statistical analysis and validated using leave-one-out cross-validation. Prieto et al. used picosecond Kerr-gated Raman spectroscopy on frozen samples of the prostate obtained at different depths during core biopsy [14]. They concluded that with the help of Raman spectroscopy and Kerr gating, it might be possible to detect the spectral differences from a small focus of adenocarcinoma of the prostate gland in an otherwise benign gland at a depth of 20 μm.

Crow et al. investigated a fiber-optic Raman system for diagnosis of bladder and prostate pathologies ex vivo, which included 38 snap-frozen prostate samples collected at transurethral resection of the prostate. Their studies have shown that this technique can be used to identify and characterize prostate adenocarcinoma ex vivo [13]. The diagnostic algorithms that they developed were able to differentiate benign prostate samples (benign prostatic hyperplasia and prostatitis) from malignant samples (prostate cancer) with an overall accuracy of 85 %.

Our research group has previously reported on clinical studies of ESS for diagnosing breast tissues, and sentinel lymph nodes [20], upper and lower GI tract mucosa [21–23], bladder [24], and melanoma [25], showing promising results. In this paper, we report on an ex vivo preliminary study of the potential for diagnosing prostate cancer based on ESS, with the goal of developing a method for optically guided biopsy to reduce sampling errors and thereby improve sensitivity, in detecting prostate cancer. As ESS uses small fiber-optic probes for performing spectroscopic measurements, the probes can be introduced into solid tissues or organs through fine needles with minimal trauma and, thus, can be integrated with core biopsies to reduce sampling error, improve sensitivity, and decrease false-negative rates. Typical spectroscopic measurements sample tissue within a few hundred microns of the probe. Our intent is to demonstrate that the spectral signatures from ESS measurements on prostate tissue exhibit repeatable differences for normal and hyperplastic glandular tissue vs. dysplastic conditions. This project should demonstrate the feasibility for performing optically guided biopsy to improve the diagnostic and therapeutic capabilities of physicians in prostate cancer. This would have important implications not only for prostate cancer diagnosis but also for guidance of interventional approaches. The long-term goal of this work is to investigate the feasibility of optical guidance techniques for in situ diagnostic and therapeutic applications in prostate disease.

Materials and methods

Measurements were made with an ESS probe on 42 freshly excised prostate glands. The ESS measurements were correlated to standard histopathological assessment, at co-registered sites of measurement, following standard fixation and staining procedures.

Prostate samples

Prostate tissue samples (205 total) were collected from radical prostatectomy specimens from 42 patients, within 30–60 min of surgical excision, from patients diagnosed with prostate cancer by prior core-needle biopsy. The patients were selected for the greatest likelihood of grossly identifiable tumor in the prostatectomy specimen. Samples are chosen without compromising clinical diagnosis or pathologic staging. The patient demographic information was not collected, as our goal was only to ascertain whether our method can discriminate between malignant and benign sites, not as a prospective study, nor with any intent to assess clinical potential across populations.

One of the key issues in this study is specimen handling for precise co-registration of spectroscopic measurements with histology. The measurement protocol is as follows: Upon receipt of the excised tissues in the pathology laboratory, the surgical margins of the fresh prostatectomy specimen are differentially inked. The specimen is symmetrically sectioned at 3–5-mm intervals in planes perpendicular to the posterior prostate surface, exposing different volumes of the gland. ESS measurements are performed on various locations of each section (mainly in the area where multiple biopsy cores containing cancer on either the right or left sides were taken). The opposite surface of each section (opposite to the side where ESS measurements were taken) is colored so the pathology reading can be done on the ESS-exposed surface. An average of five sites on each gland is examined. Each examined site was removed (using a new biopsy probe design described below) and placed in separate cassette for standard pathological assessment.

ESS system

The general principles of elastic scattering spectroscopy and the operating features of the optical system have been described in earlier publications [8, 23, 24]. The fiber-optic probe consists of two silica–silica adjacent fibers (Polymicro Technologies, LLC, Arizona, USA), one for illumination (400-μm-core diameter) and the other for collection (200-μm-core diameter). The UV–visible spectroscopic system uses an S2000 Ocean Optics spectrometer (Ocean Optics, Florida, USA) and a pulsed broadband 20-Watts-Xenon arc lamp (LS-11301, Perkin Elmer Optoelectronics, Massachusetts, USA) as the light source, resulting in a system response that covers a useful spectral range of 330–760 nm. Contribution from autofluorescence was neglected as the signal was <0.2 % of the ESS signal, and masked by noise.

For each site on the prostate gland sections, three to five measurements were taken. The number of pulses for each measurement was adjusted to cover 80 % of the dynamic range of the 12-bit CCD of the spectrometer. Tissue samples from the precise sites on the gland section, where the ESS measurements were taken, were then removed for the histopathological assessment. For each measurement, two spectra were acquired with and without triggering the light source to enable background subtraction. The average of at least three measurements was then used to represent the ESS spectrum of the examined site. The spectral response of the system was calibrated by recording a reference spectrum from a spectrally flat diffuse reflector (Spectralon®). Thus, output spectra were calculated according to:

$$I(\lambda) = \frac{I(\lambda)_{\text{tissue}} - I(\lambda)_{\text{tissue background}}}{I(\lambda)_{\text{ref}} - I(\lambda)_{\text{ref background}}}$$

Optical probe design

The probe, shown in Fig. 1, incorporates two silica–silica optical fibers, of 400- and 200-μm-core diameters, for illumination and collection, respectively, with a center-to-center separation of 350 μm.

The numerical aperture (NA) in air for both fibers is 0.22. The cladding thickness is 20±9 for the 400-μm-core diameter fiber and 10±4 for the 200-μm-core diameter fiber. A concentric tube (3-mm ID) with a sharp tip surrounds the probe core and is used as a cutting tool for the tissue sample. Once the optical measurement is taken, the external tube is advanced to remove the tissue sample in the exact location of the measurement. The sample is secured to the probe tip by means of three metal spikes incorporated in the probe core. These spikes serve a dual function: (1) preventing the movement of the probe while the measurement is taken; (2) holding the tissue sample after it is cut, to be placed in a biopsy cassette for histopathological assessment. This tool design assures accurate co-registration of tissue site for ESS measurement and histopathology assessment.

The spectra are taken with the fiber-probe tip in optical contact with the tissue surface. At this small source-detector separation, the collected light is highly sensitive to scattering but is also sensitive to the stronger absorption features of tissue [24, 26], predominantly hemoglobin and oxyhemoglobin. With this configuration, collected scattered light undergoes one to several scattering events at a typical depth (in the UV–visible region) of between 200 and 600 μm, from the surface of the tissue. For the specific probe geometry used in this work, our Monte Carlo simulations show that collected photons from tissue come from a volume of approximately 0.06 mm^3, from the typical "banana"-shaped zone of the scattered photons between the illumination and the collection fibers [27]. The propagation of the photons within the medium was determined with a reduced scattering coefficient (μ_s') of 10 cm^{-1}, an absorption coefficient (μ_a) of 0.1 cm^{-1} and a mean cosine of scattering angles (g) of 0.9 with modified Henyey Greenstein (MHG) phase function.

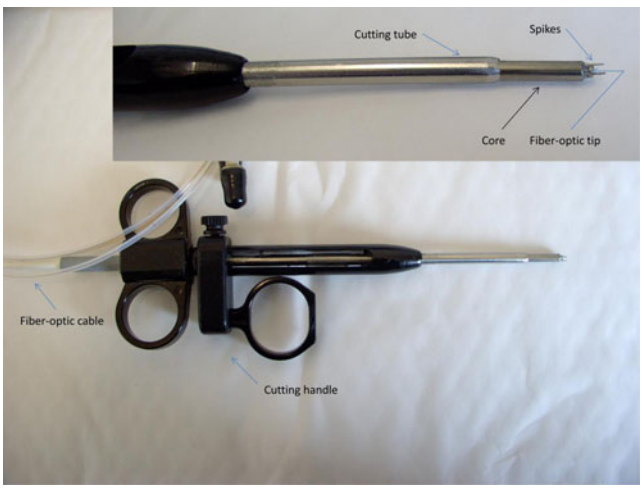

Fig. 1 Image of the customized probe used to insure co-registration of the spectral and pathology readings

Histopathology

The tissue samples were processed with standard methods in the pathology laboratory of the Boston Medical Center following spectroscopy ESS measurements. The specimens were processed and embedded in paraffin so that the planes of sectioning are defined. Sections were stained with hematoxylin and eosin for evaluation. A total of 205 prostate sites from 42 prostate glands were measured with ESS. Histopathology examination classified 136 sites as benign prostatic tissue (BPT), 34 as prostatitis (Pros), 9 as prostatic intra-epithelial neoplasia and high-grade prostatic intra-epithelial neoplasia, and 26 as prostatic adenocarcinoma.

Data analysis

The endpoints of this data analysis are the sensitivity and specificity of spectroscopy-based diagnoses, compared with routine histopathologic assessment, which is considered to be the gold standard. Each ESS spectrum consists of ~900 elements over the 330–760-nm wavelength range. Before analysis, the spectra are subjected to preprocessing in order to reduce noise and normalization to account for variations in intensity, since our analysis is based only on the spectral shape. After smoothing, cropping, and normalization, the resulting spectrum consists of 126 wavelength bands in the range of 330–760 nm. To classify the measured spectra we used pattern recognition and machine learning methods to develop a diagnostic algorithm to differentiate the different pathologies of interest. Given the high dimensionality of the data, we used an approach of an initial dimensionality reduction step, followed by classification. Dimensionality reduction was accomplished using principal component analysis [28]. For classification, a linear support vector machine (SVM) classifier was used [29, 30]. Leave-one-out cross-validation was used to obtain performance estimates of sensitivity, specificity, error rate, positive predictive value, and negative predictive values (NPV).

Results and discussion

As mentioned above, 205 individual sites from 42 prostate glands were measured with ESS. For analysis, the sites were grouped into three categories based on the grade of the histopathology as follows:

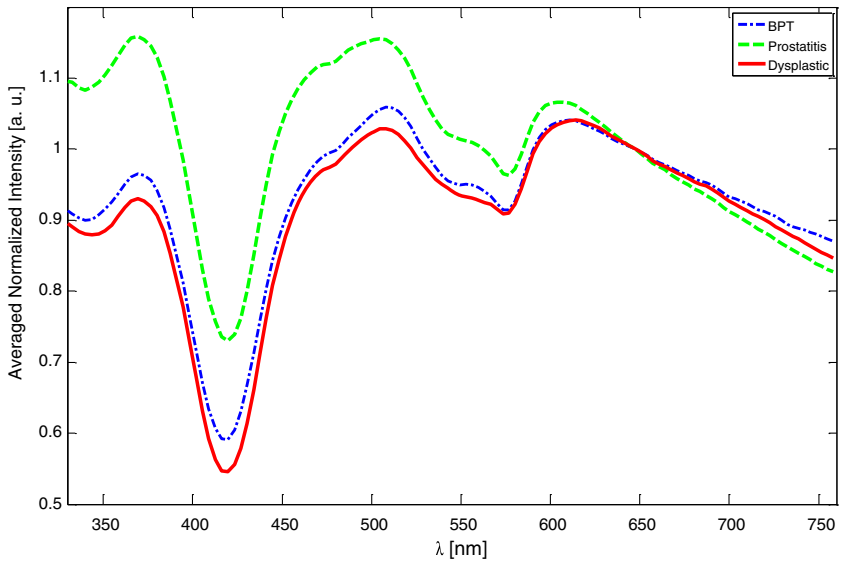

Fig. 2 ESS spectra obtained from prostate specimens ex vivo. The probe has a 350-μm separation between the excitation and collection fibers. *Bold dashed line*: prostatitis, atrophy, and inflammatory prostate tissues (n=34); *thin dot-dashed line*: BPT/BPH (benign prostatic tissue/hyperplasia, n=136); *solid bold line*: prostatic intra-epithelial neoplasia, high-grade prostatic intra-epithelial neoplasia and prostatic adenocarcinoma (dysplastic, n=35)

- Benign prostatic tissue BPT/benign hyperplasia BHP, (BPT, n=136);
- Prostatitis, atrophy, and inflammatory prostate tissues (pros, n=34);
- Dysplastic that includes prostatic intra-epithelial neoplasia, high-grade prostatic intra-epithelial neoplasia, and prostatic adenocarcinoma (dysplastic, n=35).

The data sets used in this study were unbalanced with 135 BPT and 35 dysplastic samples. The subsets of dysplastic group were too small to build a diagnostic classifier. Consequently, we have developed a binary classifier to indicate the presence of malignancy for comparison with the overall sensitivity and specificity. This is particularly useful when determining the tumor margins.

Figure 2 shows the average ESS spectra for each category. For purpose of analysis and display, all traces are normalized to intensity at 650 nm, so that only spectral shape is compared. Clear differences between the diagnostic categories are visible "by inspection" of the averaged spectra, although variability within each class was large. Some of the distinguishing spectral features are related to an increase in the size distribution of the scattering centers for malignant conditions (nuclei, organelles, etc.). We also note that, on average, there is an absorption feature centered at 480 nm, which is larger for the spectra of malignant sites. To the naked eye the tumor sites had a slight yellow tinge compared with hyperplastic and normal zones of the gland. The shape of this spectral feature is consistent with the absorption spectrum of beta-carotene, a frequent constituent of lipids and cholesterol.

Analysis of spectra is performed using principal component analysis and support vector machine classification techniques. The training sets of spectroscopic results are correlated with histological findings, and statistics are obtained using leave-one-out cross-validation. The statistical performance of the algorithms is tested on all samples. Sensitivity, specificity, positive predictive value, negative predictive value, and total error, for the detection of prostate cancer are calculated. Table 1 summarizes these results.

Comparing our results with that reported in the literature [13, 15], we could conclude that the sensitivity reported here for diagnosing prostate cancer is comparable to reported values by others [13, 15]. In this work we used ESS only, while Ref. [15] reports a combination of white-light reemission and autofluorescence spectroscopy then added Raman spectroscopy. Thus, the ESS method is simpler and less costly, but achieves similar statistics. Although, Crow et al. have reported an overall accuracy of 0.85 for detecting prostate cancer using fiber-optic Raman spectroscopy, they measured only 12 malignant specimens retrospectively. Based on our study, ESS by itself could help reduce the number of false negatives when compared with conventional techniques. As stated earlier, it has been estimated that the false-negative rate of a standard sextant sampling ranges from 15 to 31 % [1–4]. With fine-needle mediation of ESS, more extensive sampling of the prostate volume is possible with reduced trauma (compared with core biopsies). Given our preliminary results, with false-negative

Table 1 Classification performance between dysplastic and non-dysplastic groups and among non-dysplastic groups

	Sensitivity	Specificity	Error rate	PPV	NPV
Dysplastic vs BPT	0.83	0.87	0.14	0.62	0.95
Dysplastic vs pros	0.80	0.88	0.16	0.88	0.81
Pros vs BPT	0.88	0.75	0.22	–	–

rates of 15–20 %, improved results of biopsy yield can be expected, with fewer cores. Our calculated NPV reaches 0.95 for dysplastic vs benign prostatic tissue (Table 1) and is also clinically relevant. Given such a high NPV, the physician can be confident that a negative ESS test is reassuring that the patient may not have the disease since there is a larger magnitude of tissue sampling than can be accomplished with traditional tissue biopsies. Furthermore, as seen in Table 1 ESS can accurately distinguish among BPT and prostatitis, which could further benefit patient care.

In summary, combining ESS with conventional techniques for performing optically guided biopsy may help to reduce sampling errors and improve sensitivity. This would have important implications not only for prostate cancer diagnosis but also for guidance of interventional approaches. The potential benefits include:

- Guidance of core biopsy and improving sensitivity by reducing sampling errors;
- Aiding brachytherapy, by verifying the placement of insertion guide needles into diseased tissue before releasing the radioactive seeds;
- Aiding surgical prostatectomy: determining tumor margins, especially to verify whether the capsule is involved (i.e., whether or not malignancy is confined to the parenchyma). Providing a real-time in situ assessment of extra-capsular malignancy (metastases) in nearby areas;
- Assessing the response of the prostate to novel treatment modalities such as photodynamic therapy, hyperthermia, or cryosurgery;

We hope to demonstrate in future clinical studies that the spectral signatures from ESS measurements on prostate tissue will exhibit reliable differences for normal and hyperplastic glandular tissue vs. and dysplastic conditions. The potential impact of such spectral signatures will be the benefits to diagnostic and surgical applications.

Conclusion

We have shown the potential to reduce the false-negative rate in ex vivo experiments. The results are encouraging, although we are mindful of the small number of cancerous samples and the unbalanced data set. In vivo studies should be performed to evaluate whether this technique, when combined with TRUS, can be successful in an intraoperative setting to detect focal cancers. We anticipate that combining both ESS and TRUS would improve the sensitivity of detecting prostate cancer.

Acknowledgments The authors would like thank the residents and employees at Boston Medical Center ENC Pathology Lab., for their help during this project: Dr. T. Williams, Dr. F. Shaves, Dr. B. Tierno, Dr. S. Aryab, R. Gedeon, and D. Zvagelsky.

References

1. Flanigan RC, Catalona WJ, Richie JP, Ahmann FR, Hudson MA, Scardino PT, DeKernion JB, Ratliff TL et al (1994) Accuracy of digital rectal examination and transrectal ultrasonography in localizing prostate cancer. J Urol 152(5 Pt 1):1506–1509
2. Karakiewicz PI, Bazinet M, Aprikian AG, Trudel C, Aronson S, Nachabe M, Peloquint F, Dessureault J et al (1997) Outcome of sextant biopsy according to gland volume. Urology 49:55–59
3. Keetch DW, Catalona WJ, Smith DS (1994) Serial prostatic biopsies in men with persistently elevated serum prostate specific antigen values. J Urol 151:1571–1574
4. Uzzo RG, Wei JT, Waldbaum RS, Perlmutter AP, Byrne JC, Vaughan ED (1995) The influence of prostate size on cancer detection. Urology 46(6):831–836
5. Borboroglu PG, Comer SW, Riffenburgh RH, Amling CL (2000) Extensive repeat transrectal ultrasound guided prostate biopsy in patients with previous benign sextant biopsies. J Urol 163:158–162
6. Epstein JI, Walsh PC, Sauvageot J, Ballentine Carter H (1997) Use of repeat sextant and transition zone biopsies for assessing extent of prostate cancer. J Urol 158:1886–1890
7. Stroumbakis N, Cookson MS, Reuter VE, Fair WR (1997) Clinical significance of repeat sextant biopsies in prostate cancer patients. Urology 49:113–118
8. Bigio IJ, Mourant JR (1997) Ultraviolet and visible spectroscopies for tissue diagnostics: fluorescence spectroscopy and elastic-scattering spectroscopy. Phys Med Biol 42:803–814
9. Crow P, Stone N, Kendall CA, Persad RA, Wright MPJ (2003) Optical diagnostics in urology: current applications and future prospects. BJU Int 92:400–407
10. Wagnieres GA, Star WM, Wilson BC (1998) In vivo fluorescence spectroscopy and imaging for oncological applications. Photochem Photobiol 68:603–632
11. Wells WA, Barker PE, Macaulay C, Novelli M, Levenson RM, Crawford JM (2007) Validation of novel optical imaging technologies: the pathologists' view. J Biomed Opt 12:051801
12. Tearney GJ, Brezinski ME, Bouma BE, Boppart SA, Pitris C, Southern JF, Fujimoto JG (1997) In vivo endoscopic optical biopsy with optical coherence tomography. Science 276(5321):2037–2039
13. Crow P, Molckovsky A, Stone N, Uff J, Wilson B, WongKeeSong LM (2005) Assessment of fiberoptic near-infrared Raman spectroscopy for diagnosis of bladder and prostate cancer. Urology 65:1126–1130
14. Prieto MCH, Matousek P, Towrie M, Parker AW, Wright M, Ritchie AW, Stone N (2005) Use of picosecond Kerr-gated Raman spectroscopy to suppress signals from both surface and deep layers in bladder and prostate tissue. J Biomed Opt 10:044006
15. Salomon G, Hess T, Erbersdobler A, Eichelberg C, Greschner S, Sobchuk AN, Korolik AK, Nemkovich NA et al (2009) The feasibility of prostate cancer detection by triple spectroscopy. Eur Urol 55:376–384
16. Zonios G, Perelman LT, Backman V, Manoharan R, Fitzmaurice M, Van Dam J, Feld MS (1999) Diffuse reflectance spectroscopy of human adenomatous colon polyps in vivo. Appl Opt 38:6628–6637
17. Osawa M, Niwa S (1993) A portable diffuse reflectance spectrophotometer for rapid and automatic measurement of tissue. Meas Sci Technol 4:668–676
18. Perelman LT, Backman V, Wallace M, Zonios G, Manoharan R, Nusrat A, Shields S, Seiler M et al (1998) Observation of periodic fine structure in reflectance from biological tissue: a new technique for measuring nuclear size distribution. Phys Rev Lett 80:627–630

19. Underwood JCE (2000) General and systemic pathology. Churchill Livingstone, Philadelphia
20. Bigio IJ, Bown SG, Briggs G, Kelley C, Lakhani S, Pickard D, Ripley PM, Rose IG et al (2000) Diagnosis of breast cancer using elastic-scattering spectroscopy: preliminary clinical results. J Biomed Opt 5:221–228
21. Dhar A, Johnson KS, Novelli MR, Bown SG, Bigio IJ, Lovat LB, Bloom SL (2006) Elastic scattering spectroscopy for the diagnosis of colonic lesions: initial results of a novel optical biopsy technique. Gastrointest Endosc 63:257–261
22. Lovat LB, Johnson K, Mackenzie GD, Clark BR, Novelli MR, Davies S, O'Donovan M, Selvasekar C et al (2006) Elastic scattering spectroscopy accurately detects high grade dysplasia and cancer in Barrett's oesophagus. Gut 55:1078–1083
23. Mourant JR, Bigio IJ, Boyer J, Johnson TM, Lacey JA, Bohorfoush AG, Mellow M (1996) Elastic scattering spectroscopy as a diagnostic tool for differentiating pathologies in the gastrointestinal tract: preliminary testing. J Biomed Opt 1:192
24. Mourant JR, Fuselier T, Boyer J, Johnson TM, Bigio IJ (1997) Predictions and measurements of scattering and absorption over broad wavelength ranges in tissue phantoms. Appl Optics 36:949–957
25. A'Amar OM, Ley RD, Bigio IJ (2004) Comparison between ultraviolet–visible and near-infrared elastic scattering spectroscopy of chemically induced melanomas in an animal model. J Biomed Opt 9:1320
26. Mourant JR, Bigio IJ, Jack DA, Johnson TM, Miller HD (1997) Measuring absorption coefficients in small volumes of highly scattering media: source-detector separations for which path lengths do not depend on scattering properties. Appl Optics 36:5655–5661
27. Reif R, A'Amar O, Bigio IJ (2007) Analytical model of light reflectance for extraction of the optical properties in small volumes of turbid media. Appl Optics 46:7317–7328
28. Duda RO, Hart PE, Stork DG (2001) Pattern Classification. Wiley, New York
29. Burges CJC (1998) A tutorial on support vector machines for pattern recognition. Data Min Knowl Disc 2:121–167
30. Cortes C, Vapnik V (1995) Support-vector networks. Mach Learn 20:273–297